Available online at www.sciencedirect.com
SCIENCE DIRECT®
Applied Thermal Engineering 25 (2005) 1097–1113
APPLIED THERMAL ENGINEERING
www.elsevier.com/locate/apthermeng

Power optimization of an irreversible closed intercooled regenerated brayton cycle coupled to variable-temperature heat reservoirs

Wenhua Wang [a], Lingen Chen [a,*], Fengrui Sun [a], Chih Wu [b]

[a] *Naval University of Engineering, Faculty 306, Wuhan 430033, PR China*
[b] *Mechanical Engineering Department, U. S. Naval Academy, Annapolis, MD 21402, USA*

Received 28 June 2004; accepted 27 August 2004
Available online 18 October 2004

Abstract

In this paper, power is optimized for an irreversible closed intercooled regenerated Brayton cycle coupled to variable-temperature heat reservoirs in the viewpoint of the theory of thermodynamic optimization (or finite-time thermodynamics (FTT), or endoreversible thermodynamics, or entropy generation minimization (EGM)) by searching the optimum intercooling pressure ratio and the optimum heat conductance distributions among the four heat exchangers (the hot-and cold-side heat exchangers, the intercooler and the regenerator) for fixed total heat exchanger inventory. When the optimization is performed with respect to the total pressure ratio of the cycle, the maximum power is maximized twice and the double-maximum power is obtained. Further, as the optimization is performed with respect to the thermal capacitance rate matching between the working fluid and the heat reservoir, the double-maximum power is maximized again and a thrice-maximum power is obtained. In the analysis, the heat resistance losses in the four heat exchangers, the irreversible compression and expansion losses in the compressors and the turbine, the pressure drop loss in the piping, and the effects of finite thermal capacity rate of the three heat reservoirs are taken into account. The effects of the heat reservoir inlet temperature ratio, the total heat exchanger inventory and some other cycle parameters on the cycle optimum performance are analyzed by a numerical example. The optimum results are compared with those reported in recent reference for the conceptual design of

* Corresponding author. Tel.: +86 27 83615046; fax: +86 27 83638709.
E-mail addresses: lingenchen@hotmail.com, lgchenna@public.wh.hb.cn (L. Chen).

1359-4311/$ - see front matter
doi:10.1016/j.applthermaleng.2004.08.013

a closed-cycle intercooled regenerated gas turbine nuclear power plant for marine ship propulsion. The numerical example shows that the method herein is valid and effective.

Keywords: Thermodynamic optimization; Finite-time thermodynamics; Brayton cycle; Intercooled; Regenerated; Finite thermal capacity rate; Power optimization

1. Introduction

Since the theory of thermodynamic optimization (or finite-time thermodynamics (FTT), or endoreversible thermodynamics, or entropy generation minimization (EGM)) was advanced [1–3], much work has been performed for the performance analysis and optimization of finite time processes and finite size devices [4–11]. The thermodynamic performance of closed [12–29] or open [30,31], simple [12–15,22–25,27,28,30], regenerated [16–21,29,31], and intercooled [26], endoreversible [12,13,24,26,27] or irreversible [14–23,25,28–31], Brayton cycles has been also analyzed and optimized for the power, specific power, power density, efficiency, and ecological optimization objectives with the heat transfer irreversibility and/or internal irreversibilities [12–31]. Goktun et al. [32], Erbay et al. [33] and Kaushik et al. [34] analyzed and optimized the performance of an irreversible regenerative closed Brayton cycle with isothermal heat addition. On the basis of that wok, Chen et al. [35,36] and Wang et al. [37] analyzed the performance of endoreversible [35] and irreversible [36,37] intercooled and regenerated Brayton cycles coupled constant-temperature [36] and variable-temperature [35,37] heat reservoirs, and derived the power and efficiency expressions of the cycles.

Wang et al. [37] derived the power and efficiency expressions of the cycles and analyzed the influences of the effectivenesses of the hot-and cold-side heat exchangers, the intercooler and the regenerator for the given heat conductances of the four heat exchangers and the thermal capacity rate of the working fluid, that is, for the given effectivenesses of the four heat exchangers.

In the practice design, the given heat conductances of the four heat exchangers and the thermal capacity rate of the working fluid are changeable. They can be selected by carrying out the optimization calculations for the desired objectives.

The further step of this paper beyond Ref. [37] is to optimize the power of an irreversible closed intercooled regenerated Brayton cycle coupled to variable-temperature heat reservoirs using the theory of thermodynamic optimization by searching the optimum heat conductance distributions among the four heat exchangers (the hot-and cold-side heat exchangers, the intercooler and the regenerator) for fixed total heat exchanger inventory, searching the optimal intercooling pressure ratio and the optimal total pressure ratio, and searching the optimal matching of the thermal capacitance rates between the working fluid and the heat reservoir. In the analysis, the heat resistance losses in the four heat exchangers, the irreversible compression and expansion losses in the compressors and the turbine, the pressure drop loss in the piping, and the effects of finite thermal capacity rate of the three heat reservoirs are taken into account. The effects of some cycle parameters on the cycle optimum performance are analyzed by a numerical example. The optimum results are compared with those reported in recent reference for the conceptual design of a

Nomenclature

C	thermal capacity rate (kW/K)
D	pressure recovery coefficient
E	effectiveness of heat exchanger
k	specific heat ratio
N	number of heat transfer units
p	pressure (MPa)
P	power (kW)
$\overline{P}$	dimensionless power
Q	the rate at which heat is transferred (kJ)
T	temperature (K)
U	heat conductances (kW/K)
u	heat conductance distribution

Greek symbol

η	efficiency
π	total pressure ratio
π_1	intercooling pressure ratio
τ_1	cycle heat reservoir inlet temperature ratio
τ_2	cooling fluid in the intercooler and the cold-side heat reservoir inlet temperature ratio

Subscripts

c	compressor
H,h	hot-side heat exchanger
I,i	intercooler
in	inlet
L,l	cold-side heat exchanger
max	maximum
max,2	double-maximum
max,3	thrice-maximum
opt	optimum
out	outlet
$\overline{P}_{\max}$	maximum dimensionless power of the cycle
$\overline{P}_{\max,2}$	double-maximum dimensionless power of the cycle
$\overline{P}_{\max,3}$	thrice-maximum dimensionless power of the cycle
R,r	regenerator
T	total
t	turbine
wf	working fluid
1, 2, 3, 4, 5, 6, 7, 8	state points

closed-cycle intercooled regenerated gas turbine nuclear power plant for marine ship propulsion. The numerical example shows that the method herein is valid and effective.

2. Theoretical model

An irreversible closed intercooled regenerated Brayton cycle coupled to variable-temperature heat reservoirs 1-2-3-4-5-6-1 is shown in Fig. 1. The high-temperature (hot-side) heat reservoir is considered to have thermal capacity rate (mass flow rate and specific heat product) C_H and the inlet and the outlet temperatures of the heating fluid are T_{Hin} and T_{Hout}, respectively. The low-temperature (cold-side) heat reservoir is considered to have thermal capacity rate C_L and the inlet and the outlet temperatures of the cooling fluid are T_{Lin} and T_{Lout}, respectively. The cooling fluid in the intercooler is considered to have thermal capacity rate C_I and the inlet and the outlet temperatures are T_{Iin} and T_{Iout}, respectively. The pressure drop Δp in the piping is reflected using pressure recovery coefficients, that is,

$$D_1 = p_5/p_4, \quad D_2 = p_1/p_6 \tag{1}$$

Assuming the low-and high-pressure compressors have the same efficiency η_c and the turbine efficiency is η_t, and η_c and η_t reflect the irreversibility in the non-isentropic compression and expansion processes, respectively, leads to:

$$\eta_c = (T_{2s} - T_1)/(T_2 - T_1) = (T_{4s} - T_3)/(T_4 - T_3), \quad \eta_t = (T_5 - T_6)/(T_5 - T_{6s}) \tag{2}$$

Assuming that the working fluid used in the cycle is an ideal gas with constant thermal capacity rate C_{wf}, the heat exchangers between the working fluid and the heat reservoirs, the regenerator and the intercooler are counter-flow and the heat conductances (heat transfer surface area and heat transfer coefficient product) of the hot-and cold-side heat exchangers, the regenerator and the intercooler are U_H, U_L, U_R and U_I, respectively. According to the properties of the heat transfer processes, the heat reservoirs, the working fluid, and the theory of heat exchangers, the rate (Q_H) at which heat is transferred from heat source to the working fluid, the rate (Q_L) at which

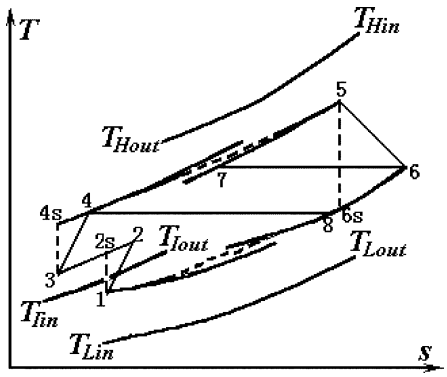

Fig. 1. T—s diagram of an irreversible closed intercooled regenerated Brayton cycle coupled to variable-temperature heat reservoirs.

heat is rejected from the working fluid to the heat sink, the rate (Q_R) of heat regenerated in the regenerator, and the rate (Q_I) of heat exchanged in the intercooler are, respectively, given by:

$$\begin{aligned} Q_H &= U_H \frac{(T_{Hin} - T_5) - (T_{Hout} - T_7)}{\ln[(T_{Hin} - T_5)/(T_{Hout} - T_7)]} \\ &= C_H(T_{Hin} - T_{Hout}) \\ &= C_{wf}(T_5 - T_7) = C_{Hmin}E_{H1}(T_{Hin} - T_7) \end{aligned} \tag{3}$$

$$\begin{aligned} Q_L &= U_L \frac{(T_8 - T_{Lout}) - (T_1 - T_{Lin})}{\ln[(T_8 - T_{Lout})/(T_1 - T_{Lin})]} \\ &= C_L(T_{Lout} - T_{Lin}) = C_{wf}(T_8 - T_1) \\ &= C_{Lmin}E_{L1}(T_8 - T_{Lin}) \end{aligned} \tag{4}$$

$$Q_R = C_{wf}(T_7 - T_4) = C_{wf}(T_6 - T_8) = C_{wf}E_R(T_6 - T_4) \tag{5}$$

$$\begin{aligned} Q_I &= U_I \frac{(T_2 - T_{Iout}) - (T_3 - T_{Iin})}{\ln[(T_2 - T_{Iout})/(T_3 - T_{Iin})]} \\ &= C_I(T_{Iout} - T_{Iin}) = C_{wf}(T_2 - T_3) \\ &= C_{Imin}E_{I1}(T_2 - T_{Iin}) \end{aligned} \tag{6}$$

where E_{H1}, E_{L1}, E_R and E_{I1} are the effectivenesses of the four heat exchangers (the hot-and cold-side heat exchangers, the regenerator and the intercooler), respectively, and are defined as:

$$E_{H1} = \{1 - \exp[-N_{H1}(1 - C_{Hmin}/C_{Hmax})]\}/\{1 - (C_{Hmin}/C_{Hmax})\exp[-N_{H1}(1 - C_{Hmin}/C_{Hmax})]\} \tag{7}$$

$$E_{L1} = \{1 - \exp[-N_{L1}(1 - C_{Lmin}/C_{Lmax})]\}/\{1 - (C_{Lmin}/C_{Lmax})\exp[-N_{L1}(1 - C_{Lmin}/C_{Lmax})]\} \tag{8}$$

$$E_R = N_R/(N_R + 1) \tag{9}$$

$$E_{I1} = \{1 - \exp[-N_{I1}(1 - C_{Imin}/C_{Imax})]\}/\{1 - (C_{Imin}/C_{Imax})\exp[-N_{I1}(1 - C_{Imin}/C_{Imax})]\} \tag{10}$$

where C_{Hmin} and C_{Hmax} are the smaller and the larger of the two capacitance rates C_H and C_{wf} respectively; C_{Lmin} and C_{Lmax} are the smaller and the larger of the two capacitance rates C_L and C_{wf}, respectively; and C_{Imin} and C_{Imax} are the smaller and the larger of the two capacitance rates C_I and C_{wf}, respectively; and N_{H1}, N_{L1}, N_R and N_{I1} are the numbers of heat transfer units of the hot-and cold-side heat exchangers, the regenerator and the intercooler, respectively, and are defined as:

$$N_{H1} = U_H/C_{Hmin}, \quad N_{L1} = U_L/C_{Lmin}, \quad N_R = U_R/C_{wf}, \quad N_{I1} = U_I/C_{Imin} \tag{11}$$

$$C_{Hmin} = \min\{C_H, C_{wf}\}, \quad C_{Hmax} = \max\{C_H, C_{wf}\} \tag{12}$$

$$C_{\mathrm{Lmin}} = \min\{C_{\mathrm{L}}, C_{\mathrm{wf}}\}, \quad C_{\mathrm{Lmax}} = \max\{C_{\mathrm{L}}, C_{\mathrm{wf}}\} \tag{13}$$

$$C_{\mathrm{Imin}} = \min\{C_{\mathrm{I}}, C_{\mathrm{wf}}\}, \quad C_{\mathrm{Imax}} = \max\{C_{\mathrm{I}}, C_{\mathrm{wf}}\} \tag{14}$$

Then the cycle power output and the cycle efficiency can be written as:

$$P = Q_{\mathrm{H}} - Q_{\mathrm{L}} - Q_{\mathrm{I}} = C_{\mathrm{wf}}(T_1 - T_2 + T_3 + T_5 - T_7 - T_8) \tag{15}$$

$$\eta = P/Q_{\mathrm{H}} \tag{16}$$

Defining the working fluid isentropic temperature ratios x and y for the low-pressure compressor and total compression process gives:

$$x = T_2/T_1 = (P_2/P_1)^m = \pi_1^m \tag{17}$$

$$y = T_5/T_6 = (P_5/P_6)^m = \pi^m \tag{18}$$

where $m = (k-1)/k$ (k is the ratio of specific heat), π_1 is the intercooling pressure ratio and π is the total pressure ratio.

Combining Eqs. (1)–(18), one can find the power of the real intercooled regenerated Brayton cycle. The dimensionless power $\overline{P}$ ($\overline{P} = P/(C_{\mathrm{L}}T_{\mathrm{Lin}})$) and the efficiency, respectively, are [37]:

$$\begin{aligned}\overline{P} = {} & \{\{1 - ABx^{-1}\eta_{\mathrm{c}}^{-2}(1 - a_2E_{\mathrm{L1}})(1 - a_3E_{\mathrm{I1}})[E_{\mathrm{R}} + C(1 - 2E_{\mathrm{R}})] - CE_{\mathrm{R}} - C(1 - E_{\mathrm{R}}) \\ & \times [a_2E_{\mathrm{L1}} + A\eta_{\mathrm{c}}^{-1}(1 - a_2E_{\mathrm{L1}})a_3E_{\mathrm{I1}}]\}a_1E_{\mathrm{H1}}\tau_1 - \{[1 - C(1 - a_1E_{\mathrm{H1}})E_{\mathrm{R}}][A\eta_{\mathrm{c}}^{-1}a_3E_{\mathrm{I1}} - 1] \\ & + ABx^{-1}\eta_{\mathrm{c}}^{-2}(1 - a_3E_{\mathrm{I1}})[E_{\mathrm{R}} + C(1 - a_1E_{\mathrm{H1}})(1 - 2E_{\mathrm{R}}) + (1 - E_{\mathrm{R}})a_1E_{\mathrm{H1}}]\}a_2E_{\mathrm{L1}} \\ & + \{1 - C(1 - a_1E_{\mathrm{H1}})E_{\mathrm{R}} - Bx^{-1}\eta_{\mathrm{c}}^{-1}(1 - E_{\mathrm{R}})a_1E_{\mathrm{H1}} - Bx^{-1}\eta_{\mathrm{c}}^{-1}[E_{\mathrm{R}} + C(1 - a_1E_{\mathrm{H1}})(1 - 2E_{\mathrm{R}})] \\ & \times [a_2E_{\mathrm{L1}} + A\eta_{\mathrm{c}}^{-1}(1 - a_2E_{\mathrm{L1}})]\}C_{\mathrm{wf}}a_3E_{\mathrm{I1}}\tau_2\}/\{\{1 - C(1 - a_1E_{\mathrm{H1}})E_{\mathrm{R}} \\ & - ABx^{-1}\eta_{\mathrm{c}}^{-2}(1 - a_2E_{\mathrm{L1}})(1 - a_3E_{\mathrm{I1}})[E_{\mathrm{R}} + C(1 - a_1E_{\mathrm{H1}})(1 - 2E_{\mathrm{R}})]\}C_{\mathrm{L}}\}\end{aligned} \tag{19}$$

$$\begin{aligned}\eta = {} & 1 - \{[a_2E_{\mathrm{L1}} + A\eta_{\mathrm{c}}^{-1}(1 - a_2E_{\mathrm{L1}})a_3E_{\mathrm{I1}}]C(1 - E_{\mathrm{R}})a_1E_{\mathrm{H1}}\tau_1 + \{[1 - C(1 - a_1E_{\mathrm{H1}})E_{\mathrm{R}}] \\ & \times [A\eta_{\mathrm{c}}^{-1}a_3E_{\mathrm{I1}} - 1] + [E_{\mathrm{R}} + C(1 - a_1E_{\mathrm{H1}})(1 - 2E_{\mathrm{R}})]ABx^{-1}\eta_{\mathrm{c}}^{-2}(1 - a_3E_{\mathrm{I1}})\}a_2E_{\mathrm{L1}} \\ & + \{Bx^{-1}\eta_{\mathrm{c}}^{-1}a_2E_{\mathrm{L1}}[E_{\mathrm{R}} + ACx^{-1}\eta_c^{-1}(1 - a_1E_{\mathrm{H1}})(1 - 2E_{\mathrm{R}})][a_2E_{\mathrm{L1}} + A\eta_{\mathrm{c}}^{-1}(1 - a_2E_{\mathrm{L1}})] \\ & + C(1 - a_1E_{\mathrm{H1}})E_{\mathrm{R}} - 1\}a_3E_{\mathrm{I1}}\tau_2\}/\{\{\{1 - ABx^{-1}\eta_{\mathrm{c}}^{-2}(1 - a_2E_{\mathrm{L1}})(1 - a_3E_{\mathrm{I1}}) \\ & \times [E_{\mathrm{R}} + (1 - 2E_{\mathrm{R}})C] - CE_{\mathrm{R}}\}\tau_1 - ABx^{-1}\eta_{\mathrm{c}}^{-2}(1 - a_3E_{\mathrm{I1}})(1 - E_{\mathrm{R}})a_2E_{\mathrm{L1}} \\ & - Bx^{-1}\eta_{\mathrm{c}}^{-1}(1 - E_{\mathrm{R}})a_3E_{\mathrm{I1}}\tau_2\}a_1E_{\mathrm{H1}}\}\end{aligned} \tag{20}$$

where $A = x + \eta_{\mathrm{c}} - 1$, $B = y + x\eta_{\mathrm{c}} - x$, $C = 1 - \eta_t + y^{-1}D\eta_t$, $D = (D_1D_2)^{-m}$, $a_1 = C_{\mathrm{Hmin}}/C_{\mathrm{wf}}$, $a_2 = C_{\mathrm{Lmin}}/C_{\mathrm{wf}}$, $a_3 = C_{\mathrm{Imin}}/C_{\mathrm{wf}}$, $\tau_1 = T_{\mathrm{Hin}}/T_{\mathrm{Lin}}$ and $\tau_1 = T_{\mathrm{Iin}}/T_{\mathrm{Lin}}$.

3. Results and discussion

3.1. General optimal performance characteristics

Eq. (19) indicates that the cycle dimensionless power $\overline{P}$ is a function of total pressure ratio π, intercooling pressure ratio π_1, heat conductance of hot-side heat exchanger U_{H}, heat conductance of cold-side heat exchanger U_{L}, heat conductance of regenerator U_{R}, heat conductance of inter-

cooler U_I and the thermal capacitance rate of the working fluid C_{wf} for the fixed boundary conditions of the cycle.

For the given U_H, U_L, U_R, U_I, and C_{wf}, that is, the given E_{H1}, E_{L1}, E_R and E_{I1}, Eq. (19) shows that there exists an optimum working fluid temperature ratio (x_{opt}) (the corresponding optimum pressure ratio is π_{opt}), which leads to the maximum dimensionless power. Wang et al. [37] analyzed the influences of E_m, E_{L1}, E_R and E_{I1} on the power output and efficiency by using Eqs. (19) and (20).

In the practice design, U_H, U_L, U_R, U_I, and C_{wf} are changeable.

For the fixed π, C_{wf} and the total heat exchanger inventory U_T(= U_H + U_L + U_R + U_I), there exist an optimal intercooling pressure ratio $(\pi_1)_{opt}$ and a group of optimal distributions among U_H, U_L, U_R and U_I, that lead to the maximum dimensionless power $\overline{P}_{max}$. Optimizing the maximum power with respect to the total pressure ratio π for the fixed C_{wf}, one can obtain the double-maximum power $\overline{P}_{max,2}$. When the optimization is performed further with respect to the thermal capacitance rate ratio C_{wf}/C_L between the working fluid and the cold-side heat reservoir, the double-maximum power is maximized again and a thrice-maximum power $\overline{P}_{max,3}$ is obtained.

For the fixed total heat exchanger inventory ($U_T = U_H + U_L + U_R + U_I$), defining:

$$u_h = U_H/U_T,\ u_l = U_L/U_T,\ u_i = U_i/U_T,\ u_r = 1 - u_h - u_l - u_i \tag{21}$$

leads to:

$$U_H = u_h U_T,\ U_L = u_l U_T,\ U_I = u_i U_T,\ U_R = (1 - u_h - u_l - u_i)U_T \tag{22}$$

Additionally, one has the constraints:

$$0 < u_h + u_l < 1,\ 0 < u_h + u_i < 1,\ 0 < u_l + u_i < 1,\ 0 < u_h + u_l + u_i < 1 \tag{23}$$

The power optimization is performed by numerical calculations, and the computational program is integrated with the optimization toolbox of MATLAB 5.3. In the calculations, $k = 1.4$, $T_{Lin} = 300\,K$, $\tau_2 = 1$, and $C_H = C_L = C_I = 1.2\,kW/K$ are set.

The characteristic of the maximum power $\overline{P}_{max}$ and its corresponding efficiency $\eta_{\overline{P}_{max}}$ versus π are shown in Fig. 2. There is an optimum total pressure ratio π_{opt} that makes $\overline{P}_{max}$ reach its climax, i.e. the double-maximum power $\overline{P}_{max,2}$. Fig. 3 shows the characteristic of $\overline{P}_{max}$ versus $\eta_{\overline{P}_{max}}$. The solid part is plotted with $1 \leqslant \pi \leqslant 60$, and in this part one can find the optimal cycle working range (in this range, both the power and its corresponding efficiency are larger). The dash part is plotted with $\pi \geqslant 60$. The curve is found to be a loop-shaped one. At the origin, both $\overline{P}_{max}$ and $\eta_{\overline{P}_{max}}$ are equal to zero. This is the same as that for an irreversible Carnot heat engine with heat resistance, heat leakage and internal irreversibility [38].

Figs. 4–7 show the characteristic of the optimum intercooling pressure ratio $(\pi_1)_{opt}$, the optimum hot-side heat conductance $(u_h)_{opt}$, the optimum cold-side heat conductance $(u_l)_{opt}$, and the optimum intercooler heat conductance $(u_i)_{opt}$ distributions at maximum dimensionless power $\overline{P}_{max}$ versus total pressure ratio π for different constant values of cycle heat reservoir inlet temperature ratio τ_1, total heat exchanger inventory U_T, compressors and turbine efficiencies η_c and η_t, and pressure recovery coefficients D_1 and D_2. From these figures, one can see that $(\pi_1)_{opt}$ increases with increases in π, U_T, η_c and η_t, and decreases with increase in τ_1 and $(\pi_1)_{opt}$ keeps almost unchangeable with increases in D_1, and D_2; $(u_h)_{opt}$ increases with increases in τ_1, U_T, η_c and η_t, D_1 and D_2, and decreases with increase in π; $(u_l)_{opt}$,increases with increase in τ_1, and decreases

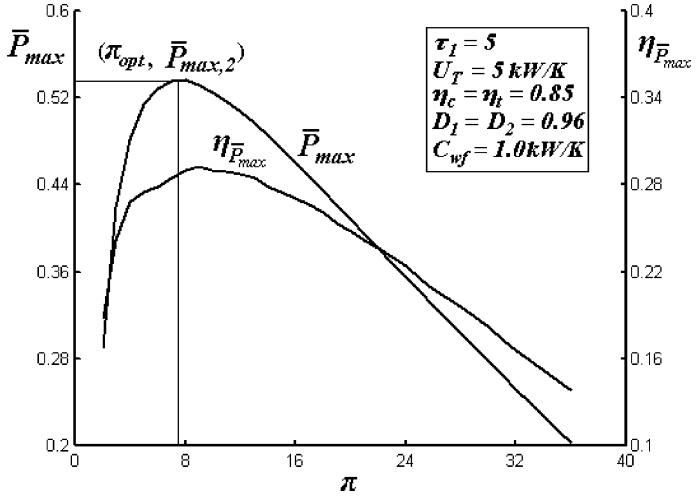

Fig. 2. Maximum power and its corresponding efficiency versus total pressure ratio.

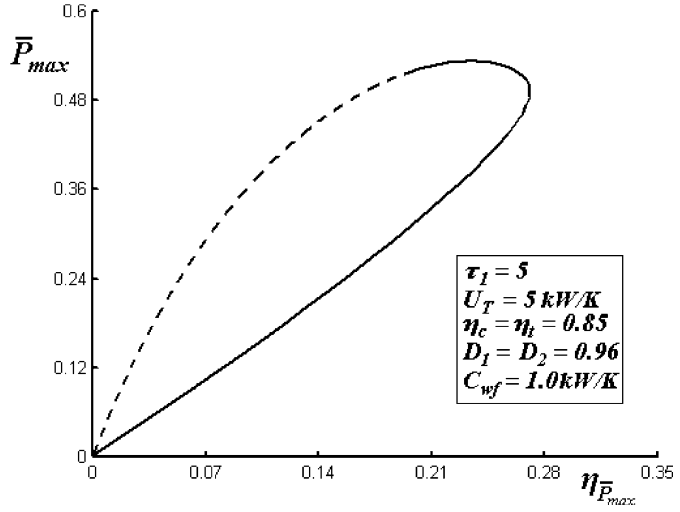

Fig. 3. Maximum power versus its corresponding efficiency.

with increases in U_T, η_c and η_t, D_1 and D_2, and at first decreases then increases as π increases; $(u_1)_{opt}$ increases with increase in π decreases with increases in U_T, η_c and η_t, D_1 and D_2, and keeps almost unchangeable with increases in D_1 and D_2.

Fig. 8 shows the characteristic of the double maximum power $\overline{P}_{max,2}$ and its corresponding efficiency $\eta_{\overline{P}_{max,2}}$ versus the cycle heat reservoir inlet temperature ratio τ_1. The corresponding optimum total pressure ratio is π_{opt}. As τ_1 increases $\overline{P}_{max,2}$, $\eta_{\overline{P}_{max,2}}$ and π_{opt} all increase nearly linearly.

Fig. 9 shows the characteristic of the double-maximum power $\overline{P}_{max,2}$ and its corresponding efficiency $\eta_{\overline{P}_{max,2}}$ versus the heat exchanger inventory U_T. As U_T increases, $\overline{P}_{max,2}$, $\eta_{\overline{P}_{max,2}}$ and π_{opt} all increase. While U_T exceeds some value increases less.

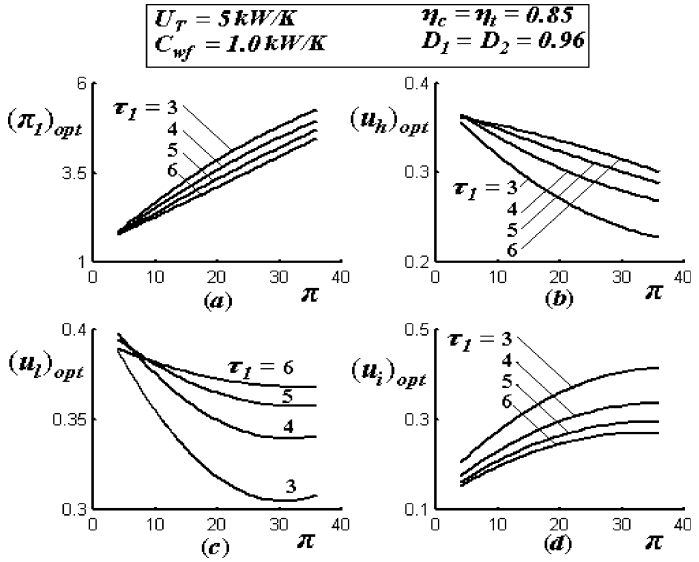

Fig. 4. Optimum intercooling pressure ratio (a), optimum hot-side heat conductance (b), optimum cold-side heat conductance (c) and optimum intercooler heat conductance (d) distribution versus total pressure ratio and cycle heat reservoir inlet temperature ratio.

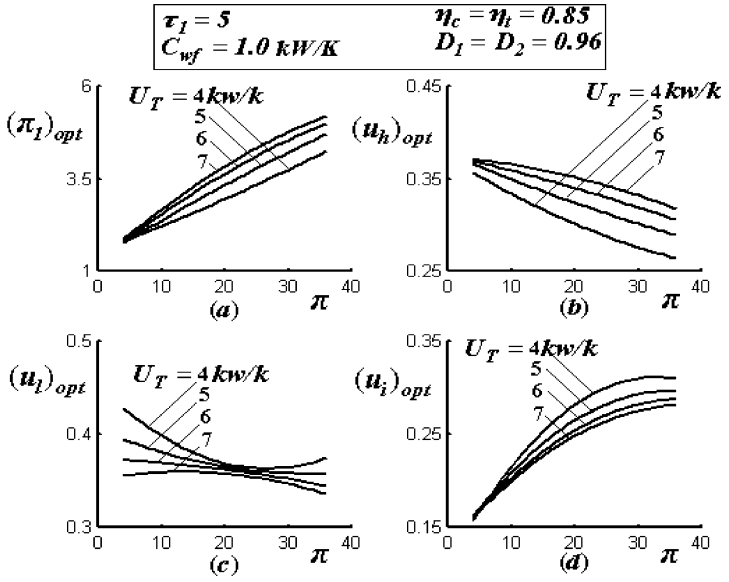

Fig. 5. Optimum intercooling pressure ratio (a), optimum hot-side heat conductance (b), optimum cold-side heat conductance (c) and optimum intercooler heat conductance (d) distribution versus total pressure ratio and heat exchanger inventory.

Fig. 10 shows the characteristic of the double-maximum power $\overline{P}_{\max,2}$ and its corresponding efficiency $\eta_{\overline{P}_{\max,2}}$ versus thermal capacity rate matching $C_{\mathrm{wf}}/C_{\mathrm{L}}$ between the working fluid and

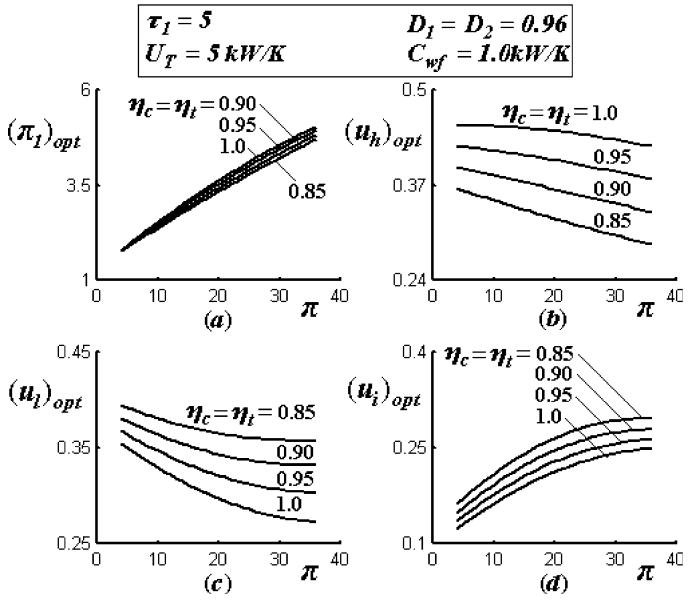

Fig. 6. Optimum intercooling pressure ratio (a), optimum hot-side heat conductance (b), optimum cold-side heat conductance (c) and optimum intercooler heat conductance (d) distribution versus total pressure ratio and compressors and turbine efficiencies.

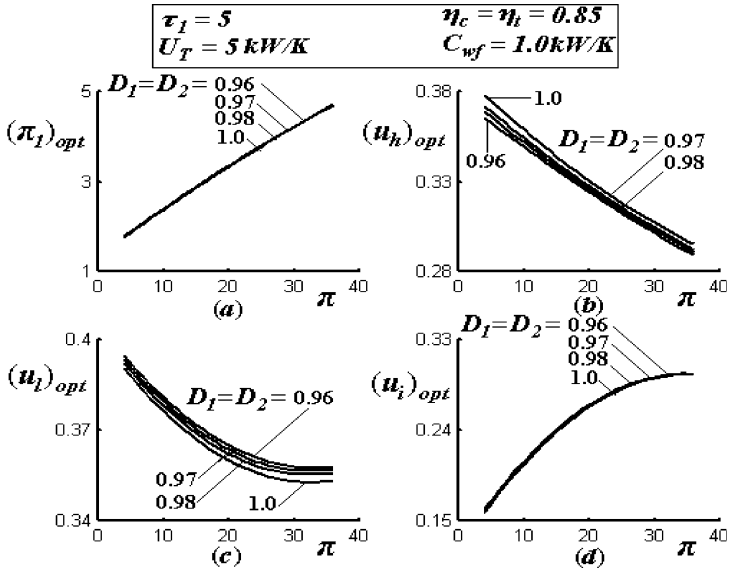

Fig. 7. Optimum intercooling pressure ratio (a), optimum hot-side heat conductance (b), optimum cold-side heat conductance (c) and optimum intercooler heat conductance (d) distribution versus total pressure ratio and pressure recovery coefficients.

cold-side heat reservoir with different C_H/C_L. It can be seen that $\overline{P}_{max,2}$ has a maximum value, i.e. the thrice-maximum power $\overline{P}_{max,3}$ as C_{wf}/C_L increases. Evidently, the efficiency corresponding to

the thrice-maximum power is not the highest. As C_{wf}/C_L increases, π_{opt} decreases at first, then increases. As C_H/C_L increases, the double-maximum power $\overline{P}_{max,2}$ and its corresponding efficiency $\eta_{\overline{P}_{max,2}}$ thrice-maximum power $\overline{P}_{max,3}$ and the corresponding efficiency, the optimal matching $(C_{wf}/C_L)_{opt}$, as well as the corresponding optimum total pressure ratio π_{opt} increase.

Fig. 11 shows the characteristic of the double-maximum power $\overline{P}_{max,2}$ and its corresponding efficiency $\eta_{\overline{P}_{max,2}}$ versus compressors and turbine efficiencies η_c and η_t. As η_c and η_t increase, $\overline{P}_{max,2}$, $\eta_{\overline{P}_{max,2}}$ and π_{opt} increase almost linearly.

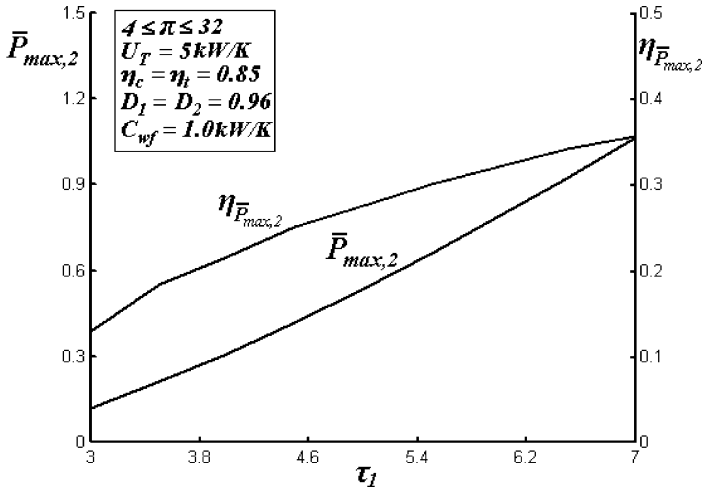

Fig. 8. Double maximum power and its corresponding efficiency versus cycle heat reservoir inlet temperature ratio.

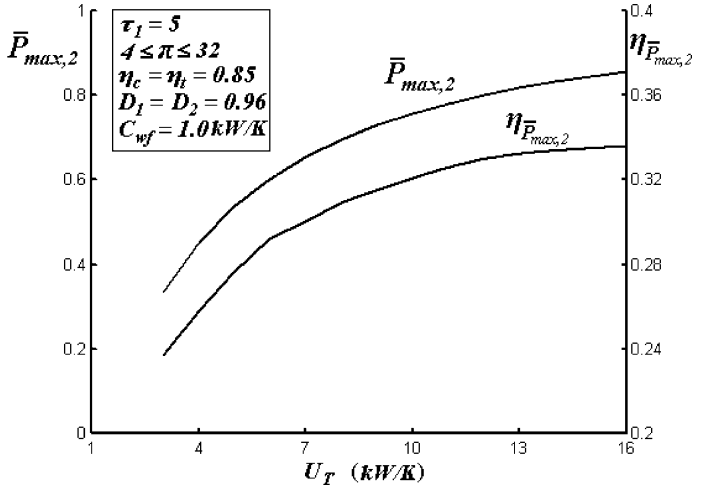

Fig. 9. Double maximum power and its corresponding efficiency versus heat exchanger inventory.

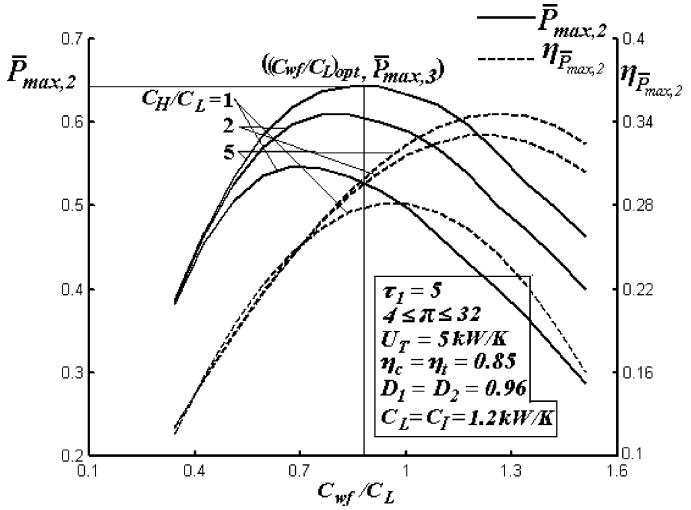

Fig. 10. Double maximum power and its corresponding efficiency versus thermal capacity rate matching between the working fluid and cold-side heat reservoir.

Fig. 12 shows the characteristic of the double-maximum power $\overline{P}_{\max,2}$ and its corresponding efficiency $\eta_{\overline{P}_{\max,2}}$ versus pressure recovery coefficients D_1, D_2. As D_1 and D_2 increase, $\overline{P}_{\max,2}$ and $\eta_{\overline{P}_{\max,2}}$ increase almost linearly, and π_{opt} keeps unchangeable.

3.2. Potential application for closed-cycle gas turbine nuclear power plant

The most of nuclear power plants are pressurized light water reactor (PWR) plants. The working fluid temperature out of the pressured-water reactor is not higher, and leads to a lower thermal-work conversion efficiency. In order to improve the efficiency and the safety, more and more

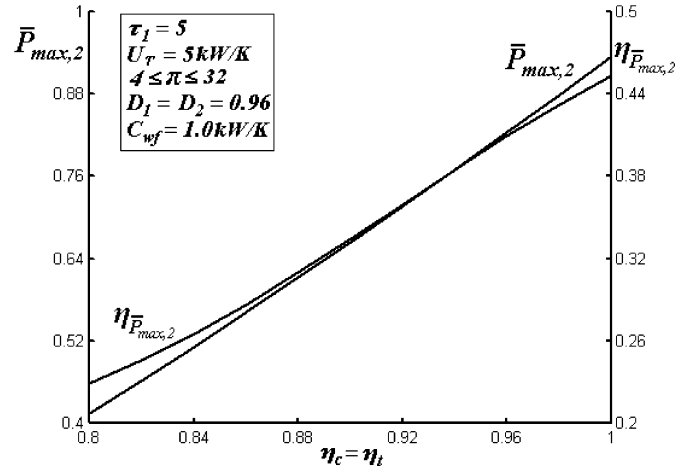

Fig. 11. Double maximum power and its corresponding efficiency versus compressors and turbine efficiencies.

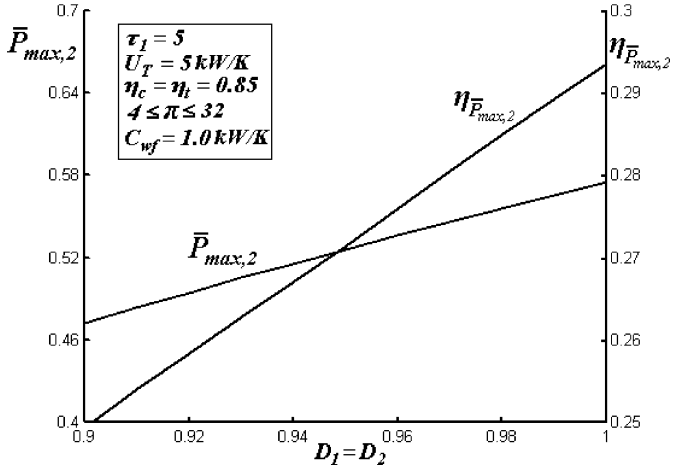

Fig. 12. Double maximum power and its corresponding efficiency versus pressure recovery coefficients.

attentions have been put to the development of high-temperature gas-cooled reactor (HTGR). This technology was proposed over forty years ago for ship propulsion [39–41] and improvements since then in nuclear fuel performance, nuclear and gas turbine materials, gas-to-gas heat exchangers and turbomachinery have made this propulsion option more attractive and achievable with existing or near-term technology [42–45].

Based on the conceptual design plan of closed-cycle regenerated helium turbine nuclear power plant for submarine provided by Gouge [45], Chen et al. [46] optimized the power, power density (defined as the ratio of power output to the maximum specific volume in the cycle) and efficiency by searching the optimum heat conductance distribution among the hot-side heat exchanger (intermediate heat exchanger) and cold-side heat exchanger (precooler) and the recuperator for the fixed total heat exchanger inventory using the theoretical results [19,28]. The optimum results are compared and consistent with those reported in Reference [45].

Gao et al. [47] provided a conceptual design plan of closed-cycle intercooled regenerated gas turbine nuclear power plant (HTGR power cycles) for marine ships.

The plant employs a primary and secondary loop similar to pressurized light water reactor power plants. The primary loop is simple in concept and includes an HTGR, a gas-to-gas heat exchanger similar to the regenerator called the intermediate heat exchanger (IHX) and a gas circulator. The IHX may have to use more conventional (and larger) heat exchanger technology than the plate fin regenerator due to the stringent leak rate requirements between the primary and secondary gas loops. The IHX is the hot-side heat exchanger of the secondary gas loop (intercooled regenerated Brayton cycle). Hot gas leaves the IHX and enters the high pressure turbine (HPT) which is driving the compressors, and then enters the low pressure turbine (LPT) which is driving a high efficiency, AC electrical generator and the propulsion motor. The lower pressure exhaust gas from the LPT enters a compact, high heat transfer regenerator (RPT) where it heats cooler gas flowing on the other side of the heat transfer surface and is itself cooled. The gas leaving the regenerator goes to another heat exchanger called a precooler (PCL) where it is further cooled by sea water before entering the low-pressure compressor. The precooler is the cold-side heat exchanger of the secondary gas loop (intercooled regenerated Brayton cycle). From the

low-pressure compressor the middle pressure gas goes through the intercooler (ICL) where it is cooled before it enters the high-pressure compressor. The high-pressure compressor raises the gas pressure to its highest value in the cycle and heats it nearly adiabatically. From the high-pressure compressor the high pressure gas goes through the regenerator as discussed above where it is pre-heated before it enters the IHX. The indirect cycle simplifies maintenance of the major propulsion plant components since all major components except the HTGR, IHX and circulator are outside the reactor compartment.

The original design parameters are shown in Table 1 [47].

The specific heats ratio, gas constant and isobaric specific heat for gas are $k = 1.4$, $R = 0.287\,\text{kJ/(kg K)}$ and $c_p = 1.0\,\text{kJ/(kg K)}$, respectively. Therefore, $C_{wf} = 79.51\,\text{kW/K}$.

For the primary loop, the thermal power produced by the reactor (P_{HTGR}) is absorbed by gas if the heat released to the ambient is negligible. Therefore, one has $P_{HTGR} = Q_H$. Solving Eq. (3) gives $C_H = 133.61\,\text{kW/K}$.

For the secondary loop, assume that the sea water inlet temperature of the precooler and the intercooler $T_{Lin} = T_{Lin} = 288.15\,\text{K}$ and the sea water temperature raise $\Delta T = 20\,\text{K}$. Moreover, solving $Q_L = C_{wf}(T_8 - T_1) = C_L\Delta T$ gives $C_L = 1338\,\text{kW/K}$. Similarly, gives $C_I = 491.5\,\text{kW/K}$. The power output of the plant is $P = P_{HTGR}\eta = 25260\,\text{kW}$.

Table 2 lists the original design values [47] and theoretical prediction values using Eqs. (19) and (20) in this paper. It can be seen that the relative error of the theoretical prediction is 6%. This fact shows that the model, method and results of this paper are reliable and provide a simplified tool for predicting the performance of practice engineering plant. They also can be applied to optimize the plant performance. The major reason produced error is that the variable specific heats characteristics of the gas is not considered in this paper. However, neglecting variable specific heats does not affect the potentials of performance analysis and optimization.

Using the known effectivenesses of IHX (E_{H1}), precooler (E_{L1}), regenerator (E_R) and intercooler (E_{I1}) and the solved the thermal capacity rates (C_H, C_L, C_{wf}), and solving Eqs. (3)–(6) gives $U_H = 220\,\text{kW/K}$, $U_L = 291.4\,\text{kW/K}$, $U_I = 29.1\,\text{kW/K}$ and $U_R = 185.5\,\text{kW/K}$. Therefore, the total heat exchanger inventory for the original design plan is $U_T = U_H + U_L + U_I + U_R = 726\,\text{kW/K}$.

For the fixed U_T, optimizing the distributions of U_H, U_L, U_I and U_R with respect to power and efficiency, respectively, gives the maximum power, the maximum efficiency and the corresponding optimal effectivenesses, as shown in Table 3.

Table 1
Original design parameters [47]

IHX effectiveness E_{H1}	0.93
Precooler effectiveness E_{L1}	0.97
Regenerator effectiveness E_R	0.70
Intercooler effectiveness E_{I1}	0.70
Compressors/turbine efficiency η_c/η_t	0.84/0.90
Pressure recovery coefficients (secondary) D_1/D_2	0.96/0.985
Pressure ratios π_1/π	3.5/17.0
Circulator power P_{cir}	1 MW
Cycle efficiency η	0.42
Reactor thermal power P_{HTGR}	60.14 MW
Mass flow rate of the working fluid $\dot{m}$	79.51 kg/s

Table 2
Comparison between the predicted and original design values

	Power (kW)	Efficiency
Original value [47]	25,260	0.42
Predicted value	23,731	0.3946
Eq. used to predict	(19)	(20)
Relative error	6%	6%

Table 3
Optimization results for power and efficiency objectives

Objective	Power (kw)	Efficiency
Maximum	26,062	0.42
Predicted value (before optimization)	23,731	0.42
Original value [47]	25,260	0.3946
Improvement by optimization	9.8%	6.4%
Optimal effectiveness corresponded to the optimization objective		
IHX effectiveness E_{H1}	0.9699	0.9921
PCL effectiveness E_{L1}	0.9298	0.9310
RPT effectiveness E_R	0.8121	0.8313
ICL effectiveness E_{I1}	0.4773	0.6411

It can be seen that the power and efficiency are increased by optimizing the heat conductances distribution. One can select the suitable ranges for the heat exchanger effectivenesses for different design optimization objectives. This will lead to improve cycle performance and to avoid the inventory resource waste.

4. Conclusion

The analysis and optimization indicates that there exist optimal intercooling pressure ratio and optimal distributions among the heat conductances of the hot-and cold-side heat exchangers, the intercooler and the regenerator for the fixed heat exchanger inventory, which lead to maximum dimensionless power. Furthermore, there exists an optimal total pressure ratio that leads to a double-maximum power output. The double maximum power has an additional maximum with respect to the thermal capacity rate matching between the working fluid and heat reservoir. The optimization of heat exchangers' heat conductance distribution for fixed total heat exchanger inventory can enhance the cycle power. An optimal cycle working range, i.e. high power output and high efficiency, can be obtained according to the characteristic of the maximum power versus its corresponding efficiency. The optimum results are compared with those reported in recent reference for the conceptual design of a closed-cycle intercooled regenerated gas turbine nuclear power plant for marine ship propulsion. The numerical example shows that the method herein is valid and effective.

Acknowledgment

This paper is supported by the Foundation for the Author of National Excellent Doctoral Dissertation of P. R. China (Project No. 200136) and the Natural Science Foundation of the Naval University of Engineering of P. R. China (Project No. HGDJJ03016).

References

[1] I.I. Novikov, The efficiency of atomic power stations, Atommaya Energiya 3 (11) (1957) 409.
[2] P. Chambadal, Les Centrales Nuclearies, Armand Colin, Paris, 1957, 41–58.
[3] F.L. Curzon, B. Ahlborn, Efficiency of a Carnot engine at maximum power output, Am. J. Phys. 43 (1) (1975) 22–24.
[4] B. Andresen, Finite-Time Thermodynamics. Physics Laboratory II, University of Copenhagen, 1983.
[5] A. De Vos, Endoreversible Thermodynamics of Solar Energy Conversion, Oxford University, Oxford, 1992.
[6] A. Bejan, Entropy generation minimization: The new thermodynamics of finite-size devices and finite time processes, J. Appl. Phys. 79 (3) (1996) 1191–1218.
[7] L. Chen, C. Wu, F. Sun, Finite time thermodynamic optimization or entropy generation minimization of energy systems, J. Non-Equilib. Thermodyn. 24 (4) (1999) 327–359.
[8] R.S. Berry, V.A. Kazakov, S. Sieniutycz, Z. Szwast, A.M. Tsirlin, Thermodynamic Optimization of Finite Time Processes, Wiley, Chichester, 1999.
[9] S. Sieniutycz, A. DeVos (Eds.), Thermodynamics of Energy Conversion and Transport, Springer, New York, 2000.
[10] C. Wu, L. Chen, J. Chen (Eds.), Recent Advances in Finite Time Thermodynamics, Nova Science Publishers, New York, 1999.
[11] L. Chen, F. Sun (Eds.), Advances in Finite Time Thermodynamics: Analysis and Optimization, Nova Science Publishers, New York, 2004.
[12] C. Wu, Power optimization of an endoreversible Brayton gas turbine heat engine, Energy Convers. Mgmt. 31 (6) (1991) 561–565.
[13] O.M. Ibrahim, S.A. Klein, J.W. Mitchell, Optimum heat power cycles for specified boundary conditions, Trans. ASME J. Engng. Gas Turbine Pow. 113 (4) (1991) 514–521.
[14] L. Chen, F. Sun, C. Wu, Performance analysis of an irreversible Brayton heat engine, J. Inst. Energy 70 (482) (1997) 2–8.
[15] M. Feidt, Optimization of Brayton cycle engine in contact with fluid thermal capacities, Rev. Gen. Therm. 35 (418/419) (1996) 662–666.
[16] C. Wu, L. Chen, F. Sun, Performance of a regenerative Brayton heat engine, Energy, Int. J. 21 (2) (1996) 71–76.
[17] L. Chen, F. Sun, C. Wu, R.L. Kiang, Theoretical analysis of the performance of a regenerated closed Brayton cycle with internal irreversibilities, Energy Convers. Mgmt. 18 (9) (1997) 871–877.
[18] L. Chen, N. Ni, G. Cheng, F. Sun, FIT performance of a closed regenerated Brayton cycle coupled to variable-temperature heat reservoirs, in: Proc. Int. Conf. Marine Engng. 3.7.1–3.7.7 Nov. 4–8, 1996, Shanghai, China.
[19] L. Chen, N. Ni, G. Cheng, F. Sun, C. Wu, Performance analysis for a real closed regenerated Brayton cycle via methods of finite time thermodynamics, Int. J. Ambient Energy 20 (2) (1999) 95–104.
[20] L. Chen, F. Sun, C. Wu, Effect of heat resistance on the performance of closed gas turbine regenerative cycles, Int. J. Power Energy Syst. 9 (2) (1999) 141–145.
[21] J.M.M. Roco, S. Veleasco, A. Medina, A. Calvo Hernaudez, Optimum performance of a regenerative Brayton thermal cycle, J. Appl. Phys. 82 (6) (1997) 2735–2741.
[22] C.Y. Cheng, C.K. Chen, Power optimization of an irreversible Brayton heat engine, Energy Sources 19 (5) (1997) 461–474.
[23] C.Y. Cheng, C.K. Chen, Efficiency optimizations of an irreversible Brayton heat Engine, Trans. ASME, J. Energy Res. Tech. 120 (2) (1998) 143–148.
[24] C.Y. Cheng, C.K. Chen, Ecological optimization of an endoreversible Brayton cycle, Energy Convers. Mgmt. 39 (1/2) (1998) 33–44.

[25] C.Y. Cheng, C.K. Chen, Ecological optimization of an irreversible Brayton heat engine, J. Phys. D: Appl. Phys. 32 (3) (1999) 350–357.
[26] C.Y. Cheng, C.K. Chen, Maximum power of an endoreversible intercooled Brayton cycle, Int. J. Energy Res. 24 (6) (2000) 485–494.
[27] L. Chen, J. Zheng, F. Sun, C. Wu, Optimum distribution of heat exchanger inventory for power density optimization of an endoreversible closed Brayton cycle, J. Phys. D: Appl. Phys. 34 (3) (2001) 422–427.
[28] L. Chen, J. Zheng, F. Sun, C. Wu, Power density optimization for an irreversible closed Brayton cycle, Open Syst. Inf. Dyn. 8 (3) (2001) 241–260.
[29] L. Chen, J. Zheng, F. Sun, C. Wu, Power density analysis and optimization of a regenerated closed variable-temperature heat reservoir Brayton cycle, J. Phys. D: Appl. Phys. 34 (11) (2001) 1727–1739.
[30] V. Radcenco, J.V.C. Vergas, A. Bejan, Thermodynamic optimization of a gas turbine power plant with pressure drop irreversibilities, Trans. ASME, J. Energy Res. Tech. 120 (3) (1998) 233–240.
[31] L. Chen, Y. Li, F. Sun, C. Wu, Power optimization of open-cycle regenerator gas-turbine power plants, Appl. Energy 78 (2) (2004) 199–218.
[32] S. Goktun, H. Yavuz, Thermal efficiency of a regenerative Brayton cycle with isothermal heat addition, Energy Convers. Mgnt 40 (12) (1999) 1259–1266.
[33] L.B. Erbay, S. Goktun, H. Yavuz, Optimal design of the regenerative gas turbine engine with isothermal heat addition, Appl. Energy 68 (3) (2001) 249–264.
[34] S.C. Kaushik, S.K. Tyagi, M.K. Singhal, Parametric study of an irreversible regenerative closed cycle Brayton heat engine with isothermal heat addition, Energy Convers. Mgnt. 44 (12) (2003) 2013–2025.
[35] L. Chen, W. Wang, F. Sun, C. Wu, Performance of a variable-temperature heat reservoir endoreversible closed intercooled regenerated Brayton cycle, in: L. Chen, F. Sun (Eds.), Advances in Finite Time Thermodynamics: Analysis and Optimization, Nova Science Publishers, New York, 2004, pp. 163–180.
[36] L. Chen, W. Wang, F. Sun, C. Wu, Closed intercooled regenerator Brayton-cycle with constant-temperature heat reservoirs, Appl. Energy 77 (4) (2004) 429–446.
[37] W. Wang, L. Chen, F. Sun, C. Wu, Performance analysis for an irreversible closed variable-temperature heat reservoir intercooled regenerated Brayton cycle, Energy Convers. Mgmt. 44 (17) (2003) 2713–2732.
[38] L. Chen, F. Sun, C. Wu, Effect of heat transfer law on the performance of a generalized irreversible Carnot engine, J. Phys. D: Appl. Phys. 32 (2) (1999) 99–105.
[39] H.F. Crouch, Nuclear Ship Propulsion, Cornell Maritime Press, Cambridge, 1960.
[40] A.W. Kramer, Nuclear Propulsion for Merchant Ships, United States Atomic Energy Commission, 1962.
[41] S. Mclain, J.H. Martens (Eds.), Reactor Handbook, second ed., Interscience, New York, 1964, pp. 704–714.
[42] C.F. McDonald, Closed-cycle gas turbine potential for submarine propulsion, ASME paper No. 88-GT-126, 1988.
[43] X.L. Yan, M.L. Lawrence, Design of closed-cycle helium turbine nuclear power plants. ASME paper No. 93-GT-196, 1993.
[44] A. Harper, J.S. Jansen, Closed Brayton cycle engine applications to emerging unmanned underwater vehicle missions, ASME paper No. 90-GT-307.
[45] M.J. Gouge, Closed cycle gas turbine nuclear power plant for submarine propulsion, Naval Engineers J. (6) (1995) 35–41.
[46] L. Chen, J. Zheng, F. Sun, C. Wu, Power, power density and efficiency optimization for a closed-cycle helium turbine nuclear power plant, Energy Convers. Mgmt. 44 (15) (2003) 2393–2401.
[47] L. Gao, R. Lin, Z. Liu, Performance comparison for three type high-temperature gas-cooled reactor power cycles, Chinese J. Engng. Thermophys. 21 (3) (2000) 273–276.